Study of $B \to \pi^- \ell^+ \nu_\ell$ Decays Using Fully Reconstructed $\Upsilon(4S) \to B\bar{B}$ Events at the Belle II Experiment

Yaroslav Kulii

München 2020

Studie von $B \to \pi^- \ell^+ \nu_\ell$ Zerfällen in vollständig rekonstruierten $\Upsilon(4S) \to B\bar{B}$ Ereignissen beim Belle II Experiment

Yaroslav Kulii

Masterarbeit

der Fakultät für Physik

der Ludwig-Maximilians-Universität

München

vorgelegt von

Yaroslav Kulii

aus Lviv

München, den 15. September

Supervisor: Prof. Dr. Thomas Kuhr

Contents

Abstract

We present the results of a study of exclusively reconstructed $B \to \pi^- \ell^+ \nu_\ell$ decays, where ℓ is an electron or a muon. Complementary B meson is reconstructed using the Full Event Interpretation algorithm. We take a piece of MC as a data and using an independent second MC sample try to analyse the method and its implications. We then try to make an estimate of the possible future Belle II analysis in terms of its performance and accuracy in measuring the branching fraction.

Chapter 1

Theoretical background

1.1 Standard Model

"Standard Model" is a name of a long-established elementary particle theory. Standard model uses the quantum field theory mathematical apparatus in explaining the current particle content and interaction. It has developed to include electroweak and strong interactions and with all the experimental results so far has been proven to be a consistent and reliable theory of particle physics. In terms of particle content, the theory consists of six quarks and six leptons, divided into three generations each, four gauge bosons and one scalar boson as one can see in figure 1. All the fermions participate in the electroweak interaction through γ, W and Z bosons, quarks participate also in the strong interaction through gluons and all the massive particles interact with the Higgs boson. The standard model as such unifies all of the mentioned distinct interactions, giving them a common mathematical framework.

The Electromagnetic interaction, being observed also on the classical level, was the first one to be described in terms of quantum field theoretical approach [1]. Development of quantum electrodynamics as a renormalizable quantum field theory was pioneering and later gave a possibility to formulate parts of the standard model using this formalism.

The "Weak interaction" got started from an attempt to describe the beta decay as an $n \to pe^{-}\bar{\nu}_e$ decay. The corresponding theory was created by

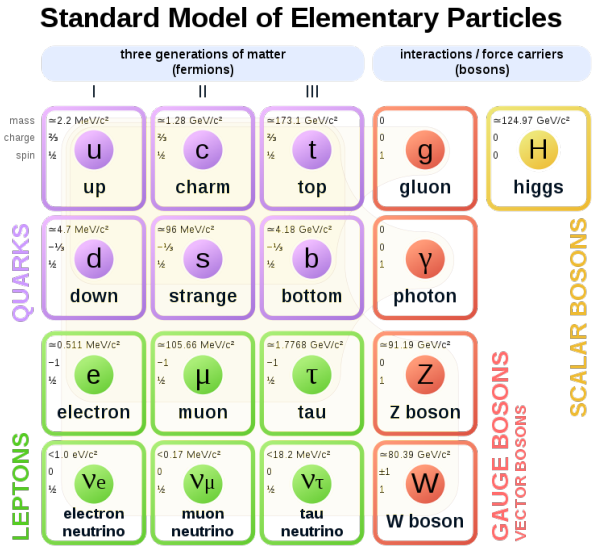

Figure 1: Particle content of the Standard Model

Enrico Fermi and is nowadays known as "Fermi theory"[2]. The motivation behind the theory at the time was the confusing energy spectrum of the outgoing electron. In the nuclear decay studied the electron was supposed to have a fixed momentum, that was expected to be represented as a sharp peak. This is because without the neutrino the decay would essentially be a two body decay. Experiment was showing quite a broad distribution, which could be explained by a missing particle, carrying some of the momentum. Even though the theory was initially criticised for introduction of an undetectably light missing particle to explain experimental results as being an ad-hoc manipulative method, it was able to describe experimental results and gave a good basis for further theoretical development.

The paradigm of a little number of basic particles (specifically proton, neutron and electron) comprising the known matter was starting to crack. In the following years discoveries of particles known now as μ lepton by Carl David Anderson and Seth Neddermeyer[3], π meson by Cecil Powell, César Lattes, and Giuseppe Occhialini [4] as well as the discovery of parity violation by Chien-Shiung Wu[5] gave a quite rich experimental background that could be used to infer a common theory. Electroweak theory was finalised in 1967 by Sheldon Glashow, Abdus Salam and Steven Weinberg[6], predicting the existence of $W^{\pm}$ and Z^0 bosons, which have not been discovered at that

moment.

The theory of strong force started it's development quite fast from the point, where development of bubble chambers and spark chambers allowed for a determination and distinction between large numbers of new hadrons. A big amount of work was carried out trying to classify the particles, for which a lot of different approaches were proposed. The first theory to propose description of smaller particles, from which hadrons were built was made in 1963 by Murray Gell-Mann and George Zweig[7, 8]. The strong sector with 6 quarks and gluons as a mediators of a strong force was developed and experimentally validated in the following two decades.

The strong interaction theory that got developed is called Quantum Chromodynamics (QCD)[9]. It's most peculiar features are colour confinement and asymptotic freedom. It introduces a quantum number technically called "colour", with stable particles composed of quarks required to be colour-neutral. Asymptotic freedom means that the interaction gets weaker on higher energy scales or correspondingly lower distance scales. The exact way in which confinement takes place is still largely a subject of research.

One specific particle, namely the Higgs boson, and its interaction should be noted separately. The Higgs boson does not incorporate any new interaction in the sense, in which electromagnetic, strong and weak interactions did as defined above, but it helps to describe mass generation. The motivation was that the electroweak theory required Z and W bosons to be massless, while those were already known to be massive. This required a separate mechanism, which was later proposed to be spontaneous symmetry breaking. Spontaneous symmetry breaking required adding another field, now called the Higgs field, quantum of which, the Higgs boson, would interact with all massive particles. The discovery of the boson in late 2012, beginning of 2013 at the Large Hadron Collider was considered a major success and yet another large confirmation of consistency of the Standard Model[10, 11].

Despite all the achievements, gravitation, existence of dark matter, neutrino oscillations and a few other phenomena (often quoted as "physics beyond the standard model") require additional modifications to be made

within the Standard Model, to be consistently described by it. Supersymmetry theories, additional mass generation mechanisms (e.g. the so-called Seesaw mechanism[12]) and other modifications are currently being developed.

1.2 CKM matrix

The Standard model lagrangian after spontaneous symmetry breaking includes a Yukawa coupling summand, that describes weak interaction of quarks with W bosons:

$$\frac{-g}{2}(\bar{u_L}, \bar{c_L}, \bar{t_L})\gamma^\mu W_\mu^+ V_{CKM} \begin{pmatrix} d_L \\ s_L \\ b_L \end{pmatrix} + h.c.,$$

where vector-column components are left-handed quark fields and vector-row components are conjugated quark fields, γ_μ are Dirac matrices and W_μ^+ is the W boson field. The *h.c.* stands for *hermitian conjugate* . The transition also involves the so-called Cabibbo-Kobayashi-Maskawa (CKM) matrix:

$$V_{CKM} = \begin{pmatrix} V_{ud} & V_{us} & V_{ub} \\ V_{cd} & V_{cs} & V_{cb} \\ V_{td} & V_{ts} & V_{tb} \end{pmatrix}$$

Amplitudes of transition from one quark to another are proportional to modules of corresponding elements of the matrix and the transition rates are correspondingly proportional to modules squared.

The Standard Model requires the CKM matrix to be unitary, for the theory to be self-consistent. After reabsorbing the common complex phase and ruling out other non-measurable parameters this leaves the CKM matrix with 4 degrees of freedom. Hence, theoretically 4 measurements are enough to determine the parameters and each further measurement puts an additional constraint and its result should be consistent with previous measurements.

$$V_{CKM} = \begin{pmatrix} 0.97401 \pm 0.00011 & 0.22650 \pm 0.00048 & 0.00361^{+0.00011}_{-0.00009} \\ 0.22636 \pm 0.00048 & 0.97320 \pm 0.00011 & 0.04053^{+0.00083}_{-0.00061} \\ 0.00854^{+0.00023}_{-0.00016} & 0.03978^{+0.00082}_{-0.00060} & 0.999172^{+0.000024}_{-0.000035} \end{pmatrix}$$

Figure 2: Current measured values of the CKM matrix [13]

The CKM matrix elements are parameters of the Standard Model and therefore are fundamentally important as such. Current experimental values can be seen in figure 2. Another interesting feature is that some beyond-standard-model theories predict breaking of unitarity in the CKM sector, making the field particularly interesting for the research.

1.3 V_{ub} and $B^0 \to \pi^- \ell^+ \nu_\ell$ decays

Main subject of this work are the $B^0 \to \pi^- \ell^+ \nu_\ell$ decays, where ℓ is either a muon or an electron. The differential decay rate equals to:

$$\frac{d\Gamma}{dq^2} = \frac{G_F^2}{24\pi^3} |V_{ub}|^2 \left| f_+\left(q^2\right) \right|^2 |\vec{p}_\pi|^3, \tag{1.1}$$

where G_F is the Fermi constant, $f_+\left(q^2\right)$ is the form factor that depends on q^2 - the four-momentum of the lepton-neutrino system.

As the decay essentially is the $b \to u$ quark transition on a quark level, it's branching fraction is proportional to $|V_{ub}|^2$. The way of measuring $|V_{ub}|$, from measuring one particular decay rate is called exclusive decay reconstruction. The value obtained with an analysis made in this way is, however, in disagreement with the inclusive decay reconstruction. The latter uses a different technique, reasoning that all the $B^0 \to X_u^- \ell^+ \nu_\ell$ decays should be considered simultaneously, as they all correspond to the $b \to u$ transition. The disagreement between the two methods is at 3σ level and is quite puzzling[14, 15].

The particular challenge in measuring $|V_{ub}|$ is the fact that the element

itself is relatively small and corresponding decays have quite a big background from other decays. V_{ub} measurements with $B \to \pi\ell\nu$ decays tend to be more precise than measurements with other exclusive decays like$B \to \rho\ell\nu$ or $B \to \omega\ell\nu$[13, 16]. Within a single analysis often a few separate exclusive decays are reconstructed and then a weighted average of the measured values for V_{ub} is taken as a final result [16].

The disagreement between inclusive and exclusive reconstruction methods and their results, possible new physics evidence and the fundamental importance in consistency of the Standard Model all together make a further research in this field an important task.

Chapter 2

Experiment description

The SuperKEKB collider is an electron-positron collider. It has been designed to be used as a B-factory, colliding the 4 GeV positron and 7 GeV electron beams at the centre of mass energy of 10.58 GeV, which corresponds to the mass of the $\Upsilon(4S)$ meson. SuperKEKB is the successor to the KEKB collider. The comprehensive upgrade of detector and accelerator systems included improvements in the magnet system, beam control systems and injector linac. The main goal pursued was to increase luminosity. It is expected to reach $8 \times 10^{35} cm^{-2} s^{-1}$, roughly 40 times higher than that of KEKB[17]. Work on the upgrade started in 2015, the detector was assembled in 2017 and early data taking started already in 2018. As of now the data taking is in progress.

A schematic description of the collider system is presented in figure 3. Electrons and positrons are first accelerated in the linac. Positrons are created and afterwards stored in the damping ring, before they can finally be injected in the final accelerator part. Fuji, Oho, Nikko and Tsukuba are four straight accelerating sections of the collider with the detector being situated at Tsukuba.

2.1 Detector

The Detector consists of a few main elements, namely the Pixel Detector (PXD), Silicon Vertex Detector (SVD), Central Drift Chamber (CDC),

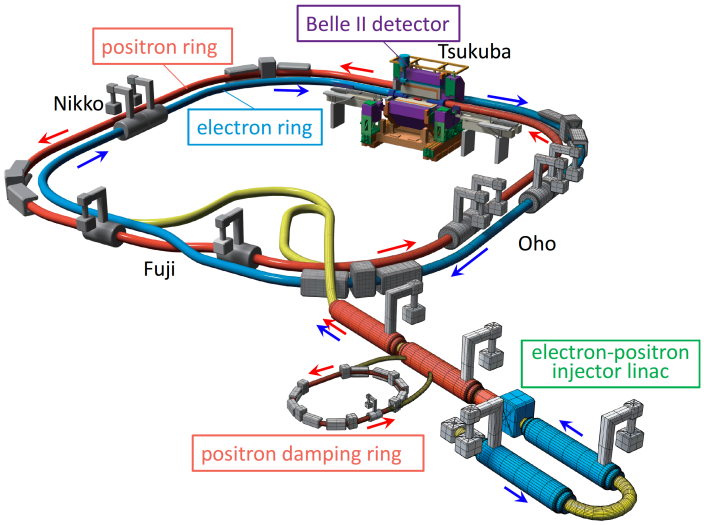

Figure 3: Schematic view of SuperKEKB

time of propagation counter (TOP), Aerogel Ring Imaging Cherenkov Detector (ARICH), electromagnetic calorimeter (ECL), K_L and muon detector (KLM) as well as other technical parts such as solenoid, triggers and data acquisition systems to state a few. An illustration is given in figure 4. Below a basic description of some of these parts is provided. An extensive description of the whole detector is given in reference [18]. In the following, detectors are listed in the order through which particles would be passing through them, that is in direction "from the beam pipe".

The PXD is the innermost detector situated right next to the beam pipe, where the collision takes place. It effectively constitutes of stripes of silicon-substrate DEPFET pixel detectors. Pixels are of the size 50×50 μm^2 and 50×75 μm^2 for inner and outer layers respectively[1]. One series of stripes is arranged in a circular-like manner, covering fully the interaction region and another series of stripes like that is also added on top, as can be seen ins figure 5. Traversing particles create electron-hole pairs, which lead to a signal, that is used for tracking of particles.

The SVD is situated around the PXD and has similar geometrical structure. It constitutes of overall 4 layers of stripe detectors surrounding the full circumference of interaction point along the beam pipe with radii 38 mm, 80

[1]Here and further by the radius a minimal distance of detector part to interaction point is meant

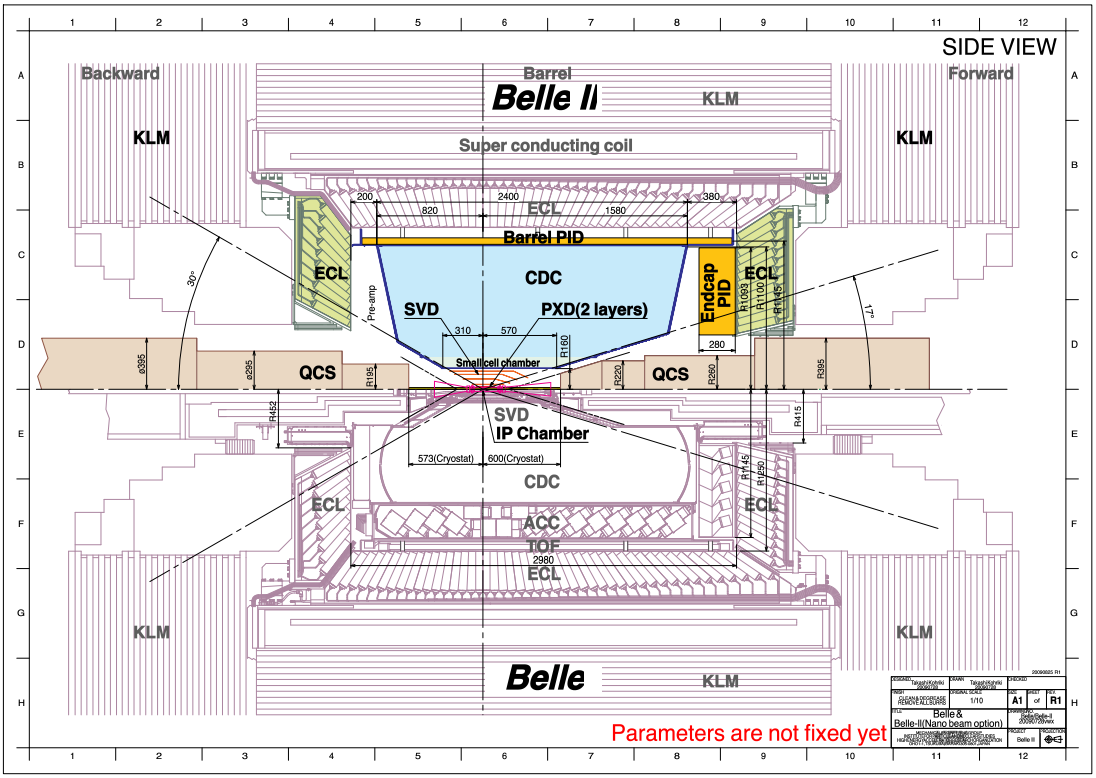

Figure 4: Schematic view of the Belle II detector. The figure was taken from a paper that described upgrade of Belle (bottom half) to Belle II (top half)[18]. Writing "Parameters are not fixed yet" refers to the fact that at the time of writing of that paper some sizes and proportions have not been approved or fixed.

mm, 115 mm and 140 mm, see figure 6. The three outer layers have their very forward sensors slanted towards the beam axis and have trapezoidal shape. The layers have 2,3,4 and 5 sensors in order from innermost to outermost. The length of each sensor is 122.8 mm. The SVD's main detecting part is made of double-sided silicon strip detectors. The pitch (distance between neighbouring stripes) is 160 μm and 50 μm for outer-side stripes and stripes on the side facing the beam pipe of innermost layer sensors. For the outer layers the same pitches are 240 μm and 75 μm, except for the trapezoidal sensors. Being farther from the interaction point than PXD, the SVD has different requirements in terms of radiation protection, resolution, sensitivity as well as several others technical limitations. In the same way, that it is in

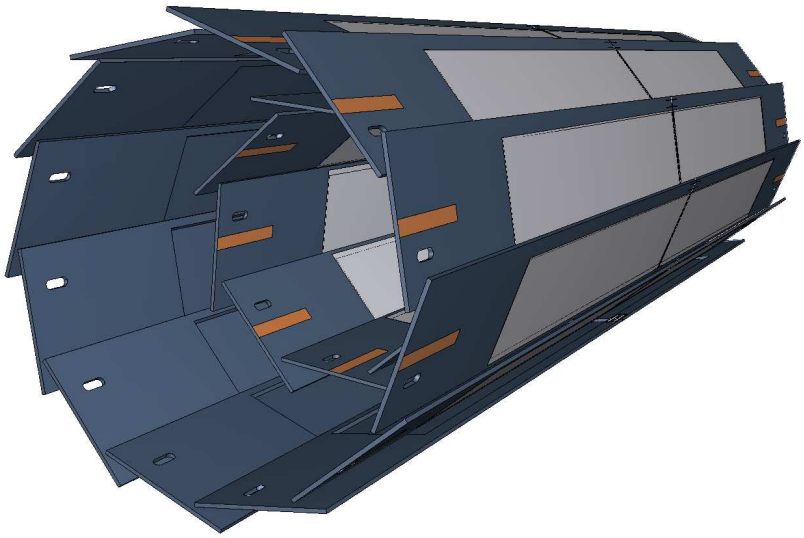

Figure 5: Schematic view of the PXD. The light grey areas are the DEPFET sensors [18]. Radii of the inner and outer layers are 14 mm and 22 mm respectively. The sensor length is 90 mm.

the PXD, traversing particles leave signals in the detector which are further used for tracking.

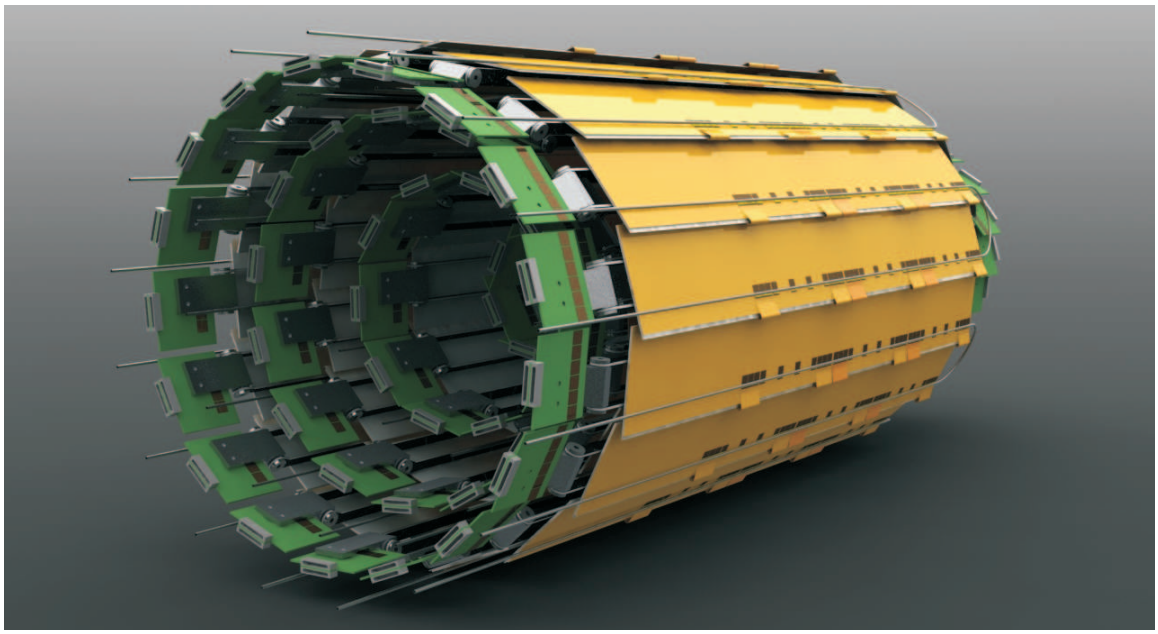

Figure 6: Schematic view of the SVD. All 4 layers are showed, each being comprised of yellow ladders consisting of several sensors [18].

Afterwards particles (or their decay products) go through the CDC.

It is a cylindrical drift chamber with a series of wires inside, configurated in layers going parallel to the beam direction or at an angle of 45.4 or 74 mrad[19]. The space between the wires is filled with a mixture of helium and ethane. When a particle passes through it ionizes gas inside and a track can be reconstructed from the signal of electrons hitting nearby anode-wires.

The particle identification system has two components, namely the barrel PID and endcap PID, situated at the central part of the detector and at the end with respect to beam axis, respectively. The barrel PID system in principle functions as time of propagation counter (TOP) for the Cherenkov radiation. Particles passing through generate Cherenkov photons, which are channelled to the photon detector through a quartz radiator. The forward endcap PID system consists of the ARICH detector that has a different structure, but effectively uses the same technique from physics point of view.

The ECL is made of 6624 CsI(Tl) scintillating crystals and is separated into barrel, forward and backward end caps. It functions basically as a calorimeter measuring the secondary particles produced in a shower.

The KLM is a K_L^0 and μ detector. It operates with the actual detecting device recording the particle showers generated by particles going through.

Chapter 3

Current state and research

As was mentioned before, measurements of the decay channels which involve $b \to u$ quark transition are hard to measure, because they have high background levels. The V_{ub} element has been measured to have a value of roughly an order of magnitude lower than V_{cb} and the branching fraction themselves are proportional to the modulus squared of the corresponding element. Therefore, it is expected that in any B-factory decays described on the quark level as $b \to u$ quark transitions are naturally expected to constitute a small fraction of all the events recorded. Whenever it comes to measurement of such branching fractions, competing methods differ, trading off statistics to purity. Exclusive decays operate with low statistics, but have relatively pure samples of data. Inclusive decay reconstructions often operate with more statistics, but have lower purity.

Reconstruction methods can be separated into two broad categories: "tagged" and "non-tagged". "Tagged" means, that in the $\Upsilon(4S) \to B\bar{B}$ event beside the B meson, that decays in a mode that is being researched, a complementary B meson is reconstructed. In the "non-tagged" analyses the complementary B meson is not reconstructed explicitly and different techniques are used. Tagged analyses operate with data that has higher purity, but is less in size, because of low reconstruction efficiency for the tag B.

As the analysis in this work is essentially a tagged exclusive reconstruction analysis, we will look at the details and results of previous such analyses in this chapter in more detail. A general description of other methods is

provided further in this chapter and a comparison of results and perspectives of different methods is presented in the chapter 9. A detailed review of mentioned methods, which has been used as a benchmark, is given in the reference [13].

Some of the previous analyses measured branching fractions only for certain q^2 intervals, with the measurement results being referred to as "partial branching fractions". In the references further no special distinction for these cases is made and measured values are referred to simply as "branching fractions".

3.1 Methodology

3.1.1 Inclusive reconstruction

Inclusive untagged reconstruction methods rely on fitting to the known theoretical predictions of the lepton momentum spectrum. Hence, they concentrate on selecting events, where leptons are appropriately reconstructed, mostly in a specific kinematic region, which gives a balance of statistical uncertainty and theoretical prediction uncertainty. In the decay $\bar{B} \to X_u \ell \bar{\nu}_l$ comprehensive selection methods are used to filter out the necessary events. The resulting spectrum is fitted to the modelled spectrum, that might include background decays (e.g. irrelevant, but present $\bar{B} \to X_c \ell \bar{\nu}_l$). Such analyses have been carried out on several independent experiments using different theoretical predictions and different suppression techniques. Early researches used overall general modeling in non-tagged analyses [20, 21, 22] and were more dependent on selection of specific region of lepton momentum. Later researches[23, 24, 25, 26, 27] tried to do a tagged analysis and reconstruct fully the complementary B meson decaying in a hadronic mode and take recoil effects into account for additional event selection.

Two specific attempts worth noting, namely [28, 29] and [27] used an additional selection for missing event momentum, judging that in a correctly reconstructed event only neutrino should be missing. Whilst in the

first case q^2 (four-momentum squared of the lepton-neutrino system) was inferred from the missing momentum and used for selection, in the second case a requirement for missing momentum squared to be consistent with zero ($-1.0 < m^2_{missing} < 0.5 GeV^2/c^4$) was used. In the sense of missing 4-momentum being interpreted as a neutrino 4-momentum for event selection and analysis, this technique is the inclusive decay analogue of the analysis presented in this thesis.

3.1.2 Exclusive reconstruction

Exclusive reconstruction relies on precise reconstruction of a lepton in a semileptonic decay mode (semileptonic, meaning that the B meson decay produces one lepton, e.g. in comparison to fully hadronic mode, where B meson decays only to hadrons). Decay modes $B^0 \to X_u \ell^+ \nu_l$ with $X_u = \pi^-, \rho^-$ and $B^- \to X_u \ell^+ \nu_l$ with $X_u = \pi^0, \rho^0, \omega, \eta, \eta'$ have been considered [16, 30, 31, 32, 33, 34, 35, 36, 37, 38, 39]. In the analyses normally a reconstruction of a charge-conjugated decay in the same manner is implied.

In an exclusive analysis a fit is performed to data in distribution of variables that are good discriminators in a given analysis. Invariant mass of ρ, ω, η mesons, missing mass squared, M_{bc}, ΔE and special variables developed specifically for a given analysis have been used[1]. Mostly simultaneous fits in multidimensional phase space are performed. With PDF simulated from a MC a fit to data is performed giving a branching fraction of a given decay mode.

The theoretical part of the analysis is mostly concerned with calculating the form factor for the given decay, to be able to calculate the $|V_{ub}|$ from the branching fraction. The form factor calculation is by itself independent from the lepton spectrum calculation done in the inclusive decays and introduces an independent set of uncertainties, making the two methods largely independent.

As was mentioned before, the exclusive reconstruction methods needs

[1] definitions of M_{bc}, ΔE is given in the chapter 5.2. M_{ES} was used in the papers of BABAR collaboration, which is an analogue of M_{bc}.

more data, but the samples have higher purity. With this the interpretation of missing momentum as a neutrino momentum is more effective and is consistently used throughout the analyses, with the technique being labelled "neutrino reconstruction" [16, 30, 34].

In a few analyses an attempt was made to do a reconstruction in a double semileptonic decay mode, e. g. with both B mesons decaying semileptonically and with two missing neutrinos in total[31, 33, 40, 41]. In these cases two neutrinos are missing and an effective neutrino reconstruction is not possible anymore. A separate discriminant variable based on the angular distribution of energy and momentum was developed to filter the events and perform the fitting. The analyses delivered results comparable in precision to those of other exclusive reconstruction methods.

Most promising results have been so far achieved in the analysis of the $B \to \pi \ell \nu_l$ decays[13]. Branching fraction for $\bar{B}^0 \to \pi^- \ell^+ \nu_l$ can be calculated from branching fraction of $B^+ \to \pi^0 \ell^+ \nu_l$ by simple multiplication by a factor of $2\tau_{B^0}/\tau_{B^+}$, so eventually study of both decays contribute to the accuracy result and were often calculated simultaneously. ρ mesons appear in similar ways in the decays of B meson and therefore constitute a considerable part of cross-feed. Cross-feed is a term to describe a process that is misinterpreted as the one being researched. In our particular case events with B meson decays to ρ meson are being misinterpreted as signal decays to π meson. This has been tackled within the fitting procedure. In the past untagged analyses have been performed, but the recent results have been exploiting tagging, reconstructing the complementary B meson in either semileptonic or hadronic mode. In the case of Belle [16] a separate tool for exclusive reconstruction of a group of hadronic and semileptonic decays of B mesons was developed. It is described further in the section 5.2.

Chapter 4

Data

The datasets used are generic Monte Carlo (MC) samples, generated by the Belle II computing group. Main analysed data is piece of generic MC that corresponds to the total integrated luminosity of $1ab^{-1}$, which includes B^+B^- and $B^0\bar{B}^0$ events, along with the so-called continuum events. A dataset of generic MC of the size that corresponds to the integrated luminosity of 500 fb^{-1} was used for selection criteria calibration and generation of distribution functions used for fitting.

Continuum events are $e^+e^- \to q\bar{q}$ events, where q is one of the c, s, u, d quarks or a τ lepton. In continuum events electron-positron collision does not result in forming a $\Upsilon(4S)$ meson, and in this analysis they constitute a background.

Additionally independently generated pieces of MC with the same structure ($e^+e^- \to q\bar{q}$ and $e^+e^- \to B\bar{B}$) were used for training of continuum suppression. Full event interpretation algorithm was trained using a mixture of MC composed of $B\bar{B}$ and B^+B^- parts of size 100 fb^{-1} each. Continuum suppression and full event interpretation are both described in the following chapter.

An algorithm, that reconstructs tracks and matches them to the calorimeter hit clusters has already been run over the datafiles after their production. The immediate files processed directly in the analysis are produced as outputs of this algorithm running over raw detector simulation data.

EvtGen[42, 43] is an event generator which also includes the framework

to add other models and generators on different stages. It was used to simulate $\Upsilon(4S)$ events and was combined with KKMC [44, 45] and PYTHIA[46] to generate continuum events. $basf2$ Belle II software[47], which uses external GEANT4 library[48, 49, 50] provided further detector simulation.

Chapter 5

Event processing

5.1 General workflow

Roughly the reconstruction algorithm has the following structure: in each event a possible $\Upsilon(4S)$ candidate is reconstructed. For this a $B^0\bar{B}^0$ meson pair has to be reconstructed. The B meson, that decays as $B^0 \to \pi^-\ell^+\nu_\ell$, is reconstructed from pion and lepton candidates. This meson is further named "signal" meson. The complementary B meson is reconstructed using an algorithm that is named Full Event Interpretation (FEI). This meson will be further on referenced as the "tag" meson. In case a few candidates pass all the selection criteria in a single event, all of them are kept. The reconstruction procedure works as described below. For the purpose of processing the events the $basf2$ software was used. The $basf2$ is a software framework developed by the Belle II collaboration.

Reconstruction operates with particle candidates. By this it is meant, that whenever a detector signal (a track or a hit cluster) is taken, it is not certain, that it is left by a given specific particle. By taking into account all the information from different detector parts a few candidates for different particles can be formed. For example, judging by the Cherenkov angle or number of hits in the KLM, of a positively charged particle may be interpreted as a π^+ or as a μ^+, giving rise to two separate candidates. For some charged particles (namely e, μ, K, π, p, d) a likelihood can be calculated of a detector signal coming from a particular particle $\mathcal{L}_{particle}$ and the particle ID

probability is defined as

$$PID\ probability \equiv \frac{\mathcal{L}_{particle}}{\Sigma_i \mathcal{L}_i},$$

where the summation over i in the denominator means summation over PID's for particles, for which a PID can be calculated (the very same e, μ, K, π, p, d).

In a single event particle lists for each separate particle are formed, that include candidates from all possible pieces of detector data in given event. When it is said, that a certain particle is reconstructed from its daughter particles, it is meant that all possible combinations of daughter particle candidates are taken, to form a list of mother particle candidates. For example, if some event has two π^- candidates and two e^+ candidates, then we will have 4 candidates for B^0 reconstructed from $B^0 \to \pi^- \ell^+ \nu_\ell$. Neutrino overall in the following analysis is considered to be missing by default. The selection criteria mentioned further are applied exactly on the particle lists mentioned.

To make sure, that a single piece of detector information is not used two times (e.g. a track is not interpreted as being a daughter particle of both signal and tag B mesons), a check is made and candidates with such duplication are discarded.

The selection criteria mentioned in this chapter are optimised by maximizing the figure of merit, which is calculated as the total number of signal candidates divided over the square root of total number of candidates. However, this requirement is not enacted strictly in all the selection criteria, to preserve more signal events in the selection. This is most often the case, when a given variable stops being a good discriminator at some point and the figure of merit has a broad plateau peak, choosing maximum of which would lead to loss of a significant part (40% and more) of the signal candidates, often increasing the figure of merit by a few percent only. This is the case for the "ΔE" variable, for example. The plots are presented in figure 9. Another reason would be that some of the variables in fact put tight restrictions and cut out a significant part of the signal canidates from the very beginning.

This would be the case for the "FEI Signal Probability" variable, for which the plots are presented in figure 10.

For the exact variables for which a selection does not strictly maximize the corresponding figure of merit the corresponding plots are given. If no such mentioning is made, it is to be assumed, that figure of merit is maximized.

Optimization was made on a MC sample, that was truth-matched. It means, that after reconstruction a check of true values was made. On the plots further the candidates are sorted into three categories: signal, non-continuum background and continuum background. Signal candidates are the candidates with both B mesons reconstructed correctly. Non-continuum background (B background) candidates are candidates from $B\bar{B}$ events with one of the B mesons reconstructed wrongly, e.g with missing final state particles, final state particles stemming from a different decay or simply wrongly reconstructed signal decay. Continuum background candidates are false B candidates reconstructed in a continuum event.

A few selection criteria of those mentioned in this chapter were introduced already on the stage of event processing in a much softer form to reduce the computational time. A separate check was made to ensure that these selection criteria did not cut off signal events (not more than a few percent). Plots and histograms presented in this chapter are generated from this reduced pre-filtered dataset.

5.2 Event selection and reconstruction

On the side of the signal B meson, pion and lepton are required to originate at the interaction point with the requirements $|d_0| < 0.4$cm and $|z_0| < 0.5$cm. The z_0 and d_0 coordinates are cylindrical system coordinates of the point of closest approach (POCA) of the particle to the interaction point. The z axis is set along the direction, opposite to that of a positron beam.

Cuts on lepton ID are made to filter out candidates that are not likely to match the mass hypothesis. By lepton ID an arithmetic sum of muon ID and

electron ID is meant. The figure of merit is given in figure 7. Additionally low

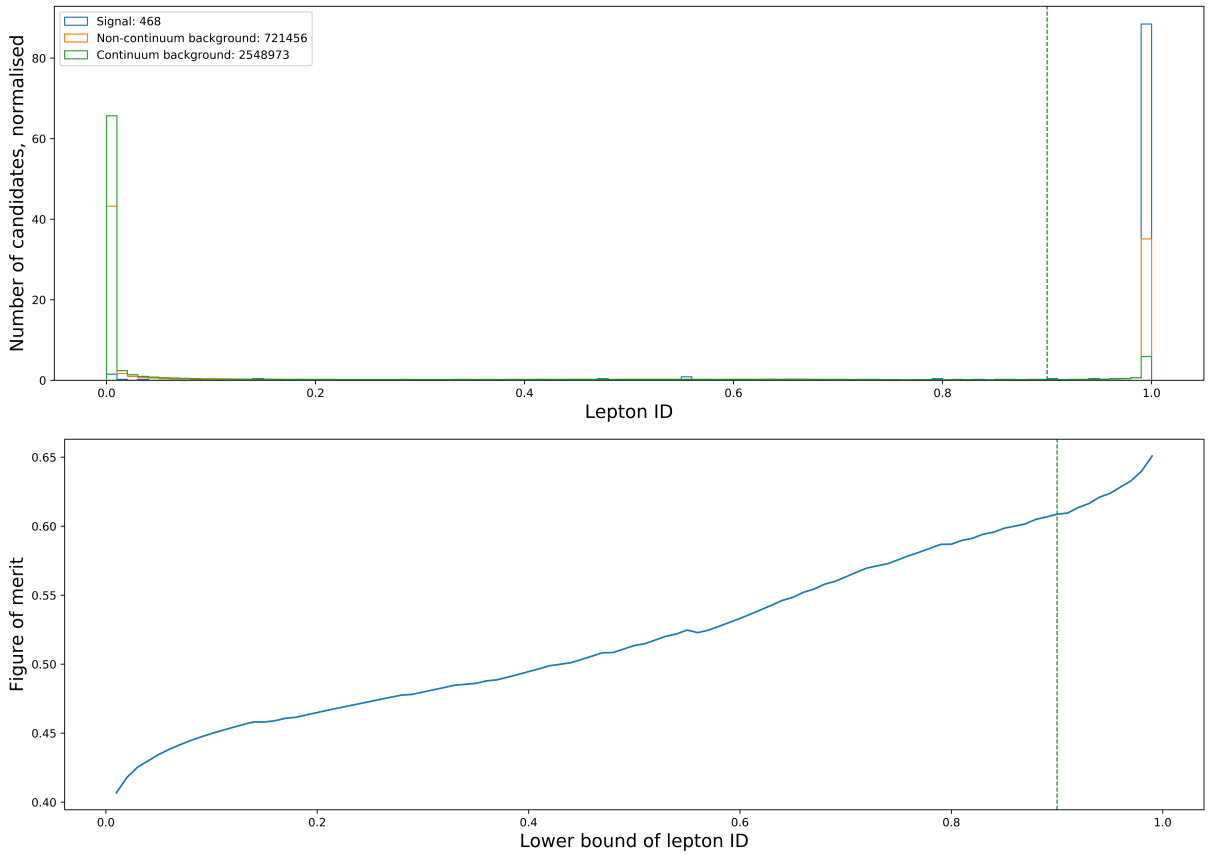

Figure 7: Distribution of lepton ID(top) and dependence of the figure of merit on the selection bound (bottom). Here and further the green dashed vertical line represents the used (upper or lower) bound value and number of the events in the distribution of the variable is normalised and given in arbitrary units. Normalisation is done so that total bin area is equal to 1.

energy leptons, that have high background due to beam effects, are filtered out, with the selection criteria $p_l > 0.3$ GeV/c. A loose cut on $cos(\theta_{YB})$ has also been put. θ_{YB} is the momentum angle between the nominal B meson and the reconstructed particle. It is calculated as:

$$cos(\theta_{YB}) = \frac{2E_B E_Y - m_B^2 - m_Y^2}{2p_B p_Y},$$

where indices Y and B indicate reconstructed particle and nominal B meson, respectively. All values are calculated in the centre of mass reference frame. E_B is taken to be equal to half of the total beam energy, which is equal to

10,579 GeV/2 = 5,2895 GeV in the centre of mass frame. For M_B the value $m_B = 5,2797$ GeV/c^2 is used[13]. p_B is calculated from E_B and M_B. The

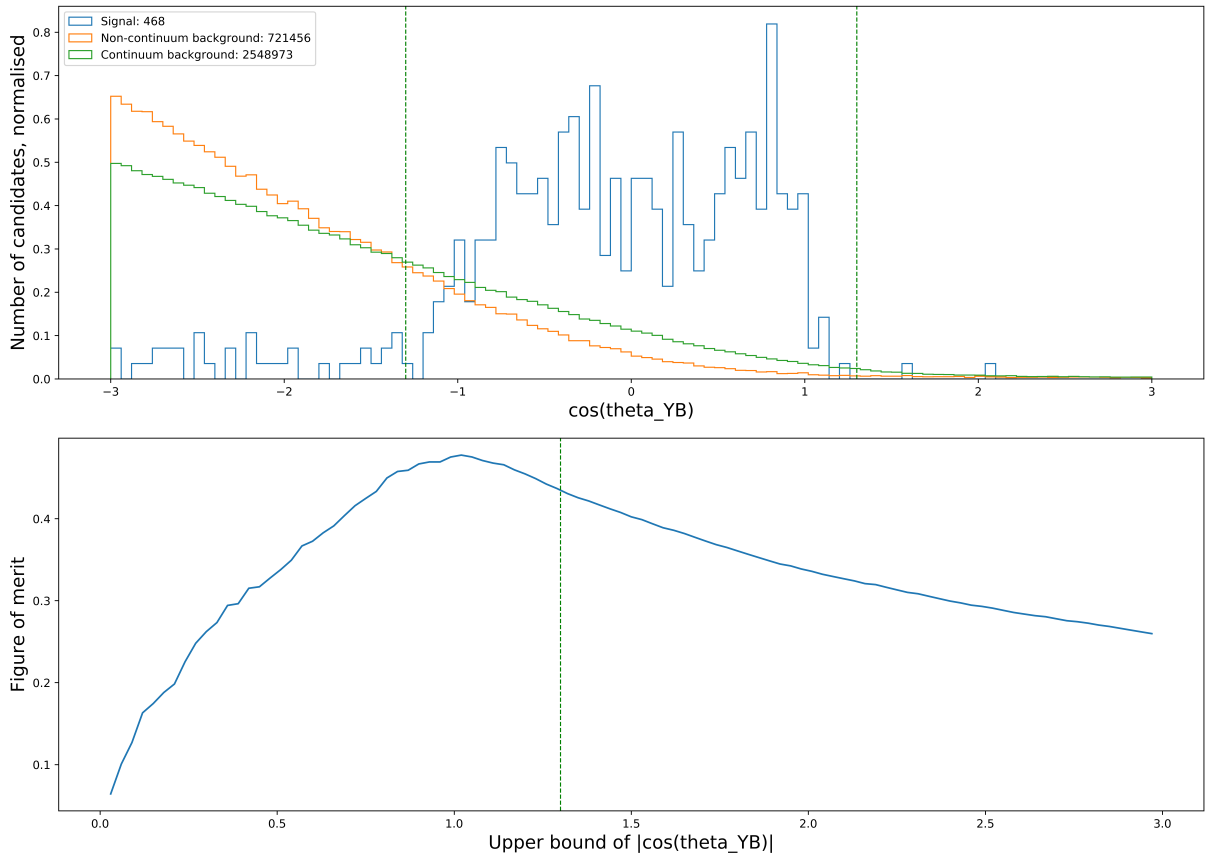

Figure 8: Distribution of $cos(\theta_{YB})$ (top) and dependence of the figure of merit on the selection bound (bottom). As one clearly sees at the bottom diagram the peak of figure of merit is around 1, but exactly putting that value as a selection boundary would cut off a 15% of the signal, whilst increasing the FOM only by a few percent. Note the different scales on two plots: FOM is plotted against the $|cos(\theta_{YB})|$, whilst the distributions are plotted against $cos(\theta_{YB})$.

angle should be in our case between -1 and 1 if a neutrino with negligibly small mass is missing. The cut has been loosened even further to account for resolution effects and missing final state radiation, see figure 8. The table 5.1 summarizes the signal side selection.

The tag-side B meson has been reconstructed in a hadronic decay mode using Full Event Interpretation (FEI)[51, 52]. FEI is an hierarchical algorithm that operates with detector information, reconstructs final state particles, intermediate resonances and finally B candidates, assigning each

$\lvert d_0(\pi,\ell)\rvert$	$<$0.4 cm
$\lvert z_0(\pi,\ell)\rvert$	$<$0.5 cm
lepton PID probability	> 0.9
p_l	> 0.3 GeV/c
$\lvert cos(\theta_{YB})\rvert$	$<$1.3

Table 5.1: List of selection criteria used for the signal B meson reconstruction.

with a probability of being correctly reconstructed. The probability is referred to as "signal probability". The algorithm has been developed from the so-called Full Reconstruction algorithm, which has been used at Belle[53]. FEI employs multivariate classifiers (MVA) that have to be trained on data samples to be used as such. Signal probability is the probability of a candidate being appropriately reconstructed as per output of the trained MVA. There is a separation, when working with FEI-reconstructed semileptonic B-meson decays and fully hadronic B-meson decays. In this work pre-trained FEI has been used to reconstruct hadronic decay modes.

The typical number of B candidates reconstructed by the FEI in a single event is quite high (on the order of a few tenths of candidates). To filter out candidates for which a final state particle is being misrecognised as not coming from a B-meson decay, a cut is made on a minimal value of M_{bc} at 5.27 GeV/c^2, and also on an absolute value of ΔE at $0,17$ GeV. The variables are defined as following:

$$M_{bc} = \sqrt{E_{beam}^2 - p_B^2},\ \Delta E = E_B - E_{beam}/2,$$

where E_{beam} refers to energy of a beam in the centre of mass frame equal to $5,285$ GeV, which is also the energy of the nominal B meson. As can be seen from the definition, M_{bc} should be equal to the mass of the B meson if the momentum has been correctly reconstructed. In the centre of mass frame B mesons should have very low momentum. Hence, any missed or wrongly associated particles should effectively increase the p_B and lower the M_{bc}. ΔE is ought to peak at 0 for a correctly reconstructed B candidate. However, the peak is in fact quite broad, see figure 9. Also, a cut on minimal signal

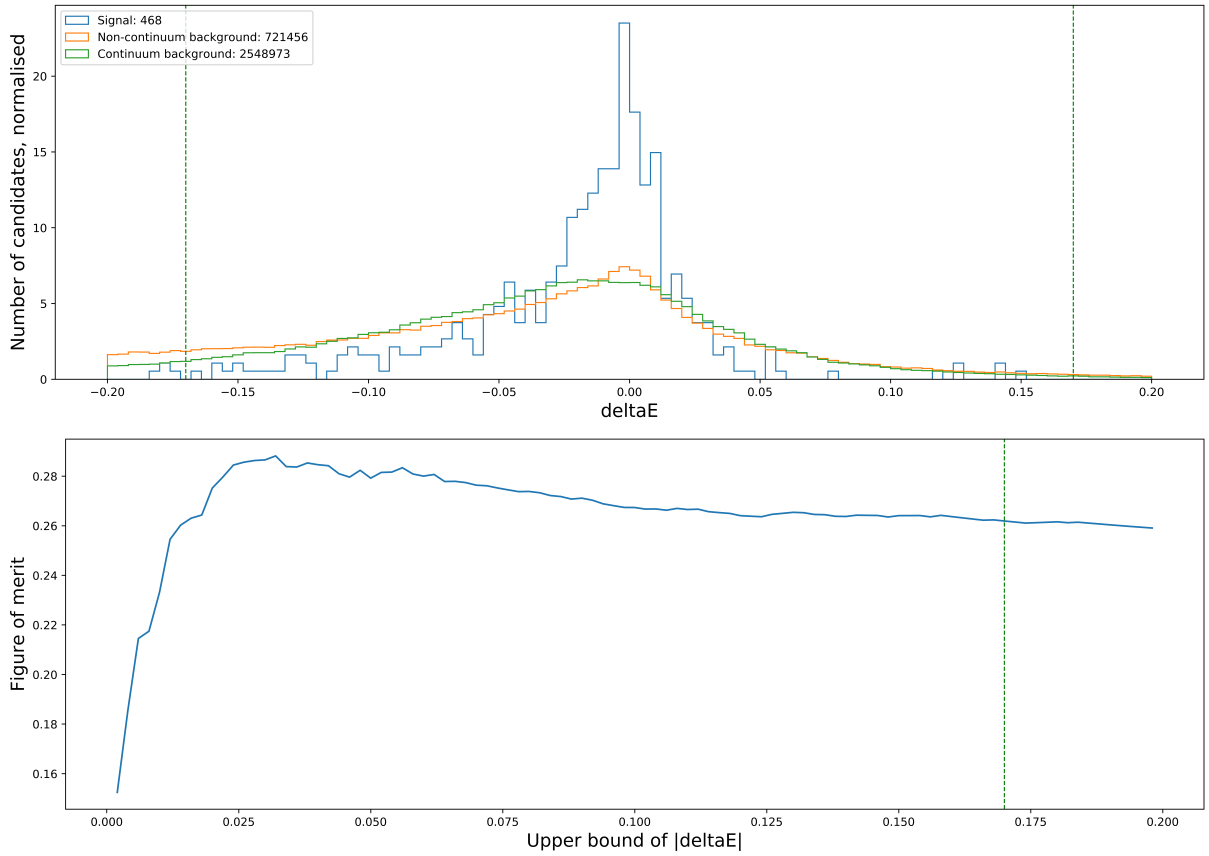

Figure 9: Distribution of ΔE (top) and dependence of the figure of merit on the selection bound (bottom). The FOM plot has a broad plateau with the FOM itself increasing from 0.26 at current boundary value to approx 0.29 at 0.03, but also filtering out 33% of the signal at that point. Due to high signal losses for relatively little rise of the FOM the selection criteria was kept quite loose.

probability is made, see figure 10. The table 5.2 summarizes the tag side selection.

$\lvert\Delta E\rvert$	$\leq$0.17 GeV
FEI Signal Probability	≥ 0.005
M_{bc}	> 5.27 GeV$/c^2$

Table 5.2: List of selection criteria used for the tag B meson reconstruction.

After we've reconstructed both tag and signal side, we combine them to reconstruct an $\Upsilon(4S)$ candidate. We do further filtering on its rest of event (ROE). ROE is a group of all objects that were not used in the reconstruction of particular candidate from corresponding particle list. In the case here

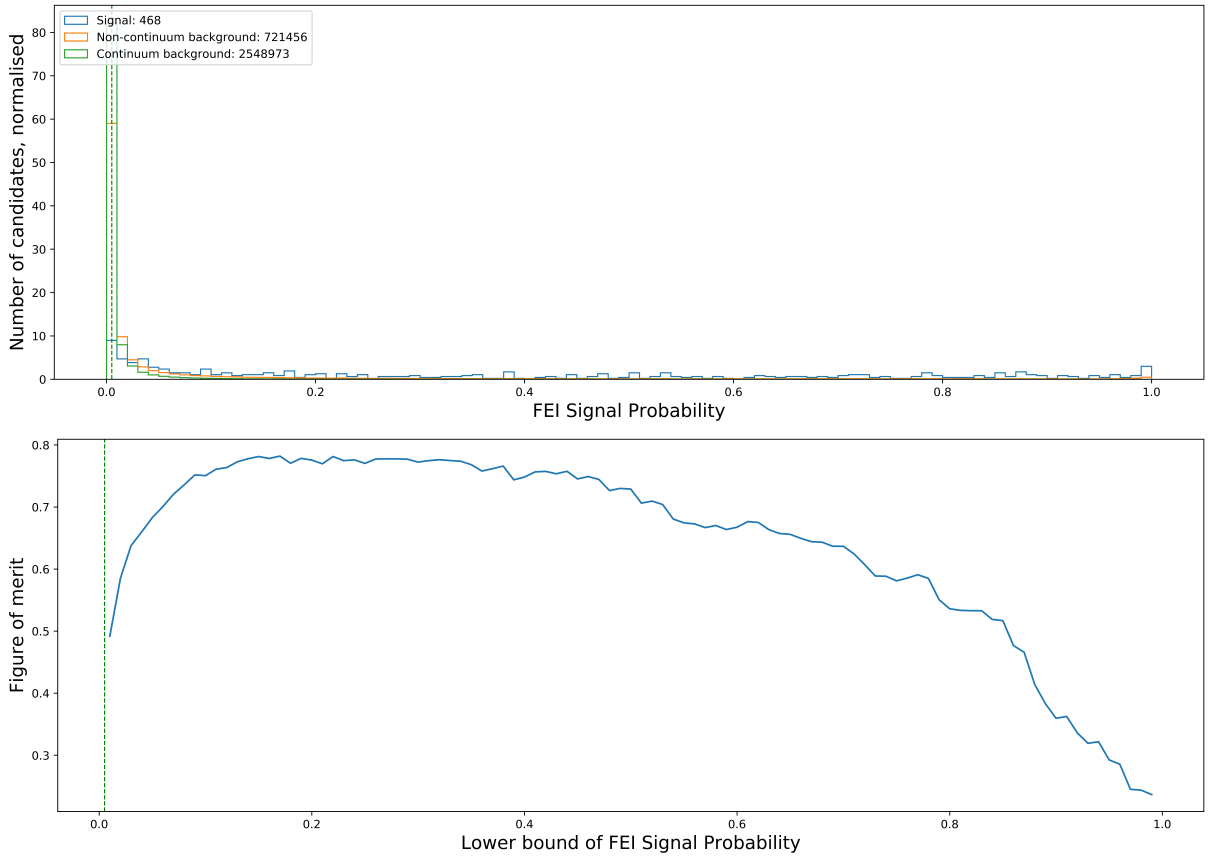

Figure 10: Distribution of FEI Signal Probability (top) and dependence of the figure of merit on the selection bound (bottom). The selection value was kept low because of big signal losses. For comparison, a limit at 0.1 would cut out 35% of the signal events, at 0.05 - 25% of the signal events.

ROE would contain tracks and hits not included in the reconstructed $\Upsilon(4S)$ candidate. We limit the maximal energy deposited in the neutral ECL cluster and number of additional tracks in the ROE, as large leftovers imply that we reconstructed the event wrongly (e.g. big amount of radiation and/or a neutral particle being missed).

R_2	<0.4
$\Upsilon(4S).ROE\_Eextra$	$\leq$ 1.5 GeV
$\Upsilon(4S).ROE\_Ntracks$	≤ 2

Table 5.3: Selection criteria used for filtering of reconstructed $\Upsilon(4S)$ candidates.

R_2 is the normalised second Fox Wolfram moment, described in the following subsection 5.3. It is used here explicitly as a separate cut, as it has

good discriminative properties and is used for that purposes on a separate instance. R_2 should not be higher than 0.4 for correctly reconstructed events with no particles missing. The table 5.3 summarizes the selections applied to a reconstructed $\Upsilon(4S)$ candidate.

5.3 Continuum Suppression

A separate step is made to get rid of continuum events (i.e. $q\bar{q}$ and $\tau^+\tau^-$). A multivariate classifier, based on boosted decision trees is trained on a sample of generic MC to discriminate between continuum and non-continuum events [54]. Since in the decay $\Upsilon(4S) \to B^0\bar{B}^0$ in the centre of mass frame B-mesons have considerably small kinematic energy, that decay is more spherical, whereas continuum events tend to be more collimated and have jet-like structure. The set of variables at the table 5.4 shows all the variables used for training the classifier. The classifier operates with a given particle list B-candidates and their rest of events.

For training the classifier a processed MC dataset was used. In the MC an FEI-reconstruction was made and tag B candidates were generated. All of the selection criteria for tag B meson mentioned above were applied. The continuum suppression classifier inside the main analysis was applied onto the reconstructed tag B meson also after the cuts on the tag B were made. In our particular case application of the continuum suppression onto the signal B meson was observed to be worse. This can be explained by the fact, that signal B meson selection is not as restrictive and preserves does not deliver a good of non-continuum events in

Two big families of variables used are KSFW moments and CLEO cones. Kakuno-Super-Fox-Wolfram moments (KSFW moments), noted as H are a modification of original Fox Wolfram moments[55]. As a complex of values they describe the topology of the event. R_2 is the normalised second Fox Wolfram moment. CLEO cones were developed by the CLEO collaboration and by definition they are the sum of projections of particle momenta, which are inside the cone, the symmetry axis being the thrust

axis. Cones numbered from 1 till 9 have an opening angle from 10^o with a step of 10^o. The thrust axis $\vec{n}_T$ is the axis, sum of projections of momenta of particles onto which is maximized. The thrust scalar T is the sum of the projections normalized to the sum of their moduli.

$$T = \max_{\vec{n}_T} \frac{\sum_i |\vec{p}_i \cdot \vec{n}_T|}{\sum_i |\vec{p}_i|}, \tag{5.1}$$

T_B and T_z are the thrust values of the signal B meson and projection of the thrust axis onto z-axis respectively. $cos(\theta_{T_B,T_O})$ and $cos(\theta_{T_B,z})$ are cosines of angles between thrust axis of B meson and and its rest of event and thrust axis of B meson and z axis respectively. mm^2 and E_t are missing mass squared and missing transverse energy. The extensive description of used variables is given in the references [56, 57]. After training the classifier and

R_2
T_B
T_z
$cos(\theta_{T_B T_O})$
$cos(\theta_{T_B z})$
E_t
mm^2
H_{00}^{so}
H_{02}^{so}
H_{04}^{so}
H_{10}^{so}

H_{12}^{so}
H_{14}^{so}
H_{20}^{so}
H_{22}^{so}
H_{24}^{so}
H_0^{oo}
H_1^{oo}
H_2^{oo}
H_3^{oo}
H_4^{oo}

CleoCone(1)
CleoCone(2)
CleoCone(3)
CleoCone(4)
CleoCone(5)
CleoCone(6)
CleoCone(7)
CleoCone(8)
CleoCone(9)

Table 5.4: Variables used for the training of the Continuum Suppression module

applying it in the analysis we get a probability of candidate being in the continuum event for each signal B meson candidate. We then make a cut on it being more than 0.2, see figure 11.

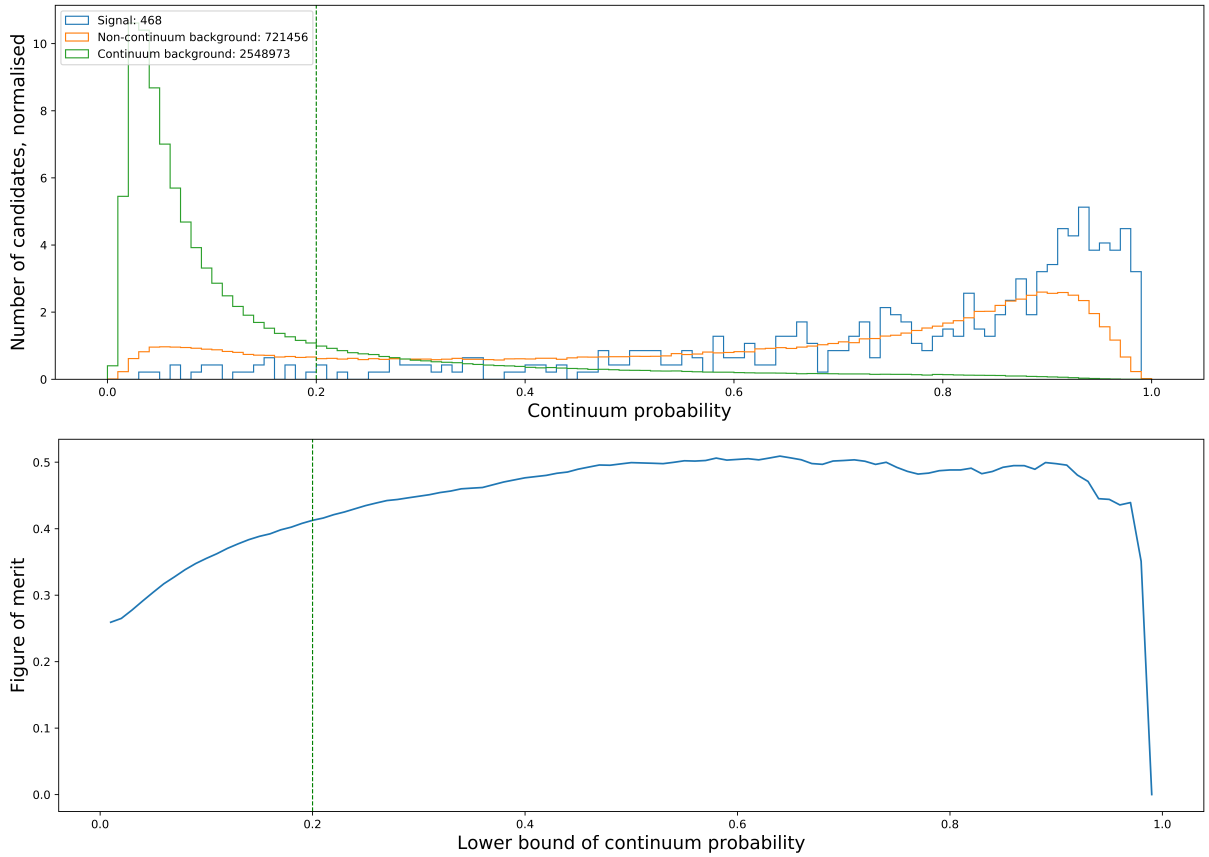

Figure 11: Distribution of continuum probability (top) and dependence of the figure of merit on the selection bound (bottom).

Chapter 6

Fitting

Once we've established a selection procedure using MC, for which we openly did truth matching (openly checked the true generated values) we can start working with data. In our case the data is a 1 ab^{-1} piece of independently generated MC. We treat this piece of MC as data, e. g. truth matching is not made and we operate solemnly with information that could be measured in the detector for a piece of true data.

Because in the real data we cannot check if certain piece of information comes from signal or background processes we perform a fit. Missing mass squared of the event is a variable, for which signal data has a distinct peak at zero, while B background and continuum background have different shapes that do not have that peak. Therefore, we fit the MC-generated probability distribution functions (PDF) to the data with the free parameters of the fit being the coefficients multiplied to the normalised PDFs, see equation 6. As the PDFs are by definition normalised to 1 the coefficient values we get after the fitting should show the amount of different candidates within the data sample.

For fitting the RooFit module of the ROOT software is used [58]. An extended binned maximum likelihood fit to the variable "missing mass squared" is performed. The components to the fit are continuum background, non-continuum background and the signal. We generate the PDFs by running the analysis on the independent sample of generic MC which corresponds to the integrated luminosity of $500 fb^{-1}$ and includes 267.5×10^6 $B^0\bar{B}^0$

$$PDf_{full} = c_1 \cdot PDF_{signal} + c_2 \cdot PDF_{Bbackground} + c_3 \cdot PDF_{continuum}$$

Figure 12: The full PDF consists of a linear combination of signal, continuum and b background PDFs, with the coefficients c1, c2 and c3 being the free parameters of the fit

events. After truth matching the separate distributions are saved. Signal, B-background and continuum distributions can be seen in figure 13.

Missing mass squared is defined in a specific way, which incorporates mass hypothesis for the signal-side B meson. The four-momentum of the B_{sig} is defined as following:

$$p_{B_{\text{sig}}} \equiv (E_{B_{\text{sig}}}/c, \vec{p}_{B_{\text{sig}}}) = c\left(\frac{m_{\Upsilon(4S)}}{2}, -\frac{\vec{p}_{B_{\text{tag}}}}{|\vec{p}_{B_{\text{tag}}}|}\sqrt{\left(\frac{m_{\Upsilon(4S)}}{2}\right)^2 - m_B^2}\right).$$

As one can see, the mass with this definition is explicitly a B-meson mass. In the calculation the recent values $m_B = 5,2797$ GeV$/c^2$ and $m_{\Upsilon(4S)} = 10,579$ GeV$/c^2$ are used[13]. The missing 4-momentum is then defined as following:

$$p_{\text{miss}} \equiv (E_{\text{miss}}/c, \vec{p}_{\text{miss}}) = p_{B_{\text{sig}}} - p_Y,$$

where p_Y is a reconstructed B-candidate 4-momentum, that is, sum of the 4-momenta of pion and lepton. Finally, missing mass squared is defined as:

$$m^2 = p^2_{\text{miss}}$$

The final PDFs used for fitting can be seen in figure 13. Continuum background shows large statistical fluctuations which can be improved in future analyses by using more statistics.

The fitted data and fit result can be seen in figure 14. Fitted coefficient values are represented at the table 6.1 and correlation coefficients are in the table 6.2.

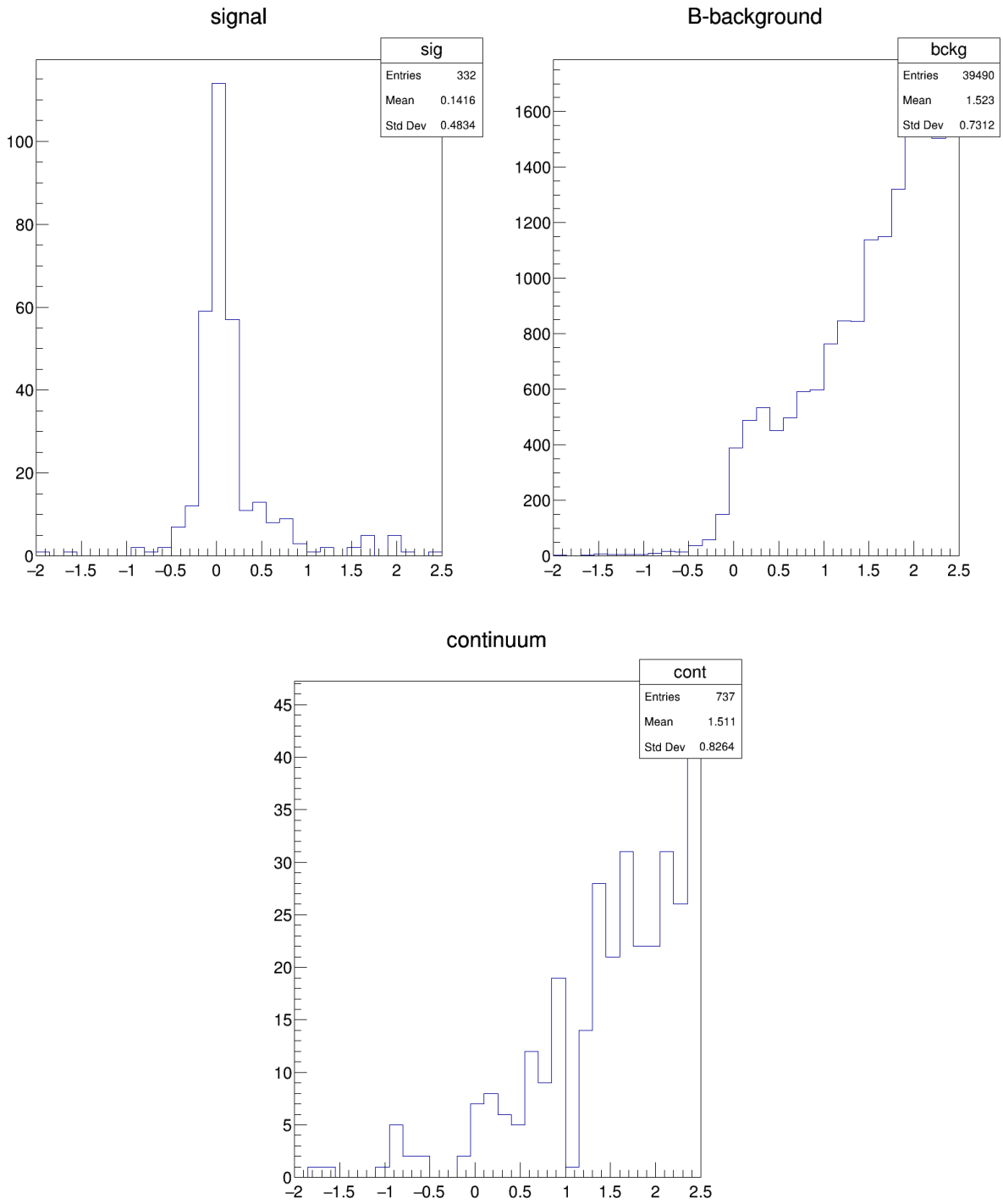

Figure 13: Distributions used for creating the PDF's. In all three cases the x axis is the missing mass squared and the y axis is the number of candidates. PDFs are generated through normalisation of these distributions.

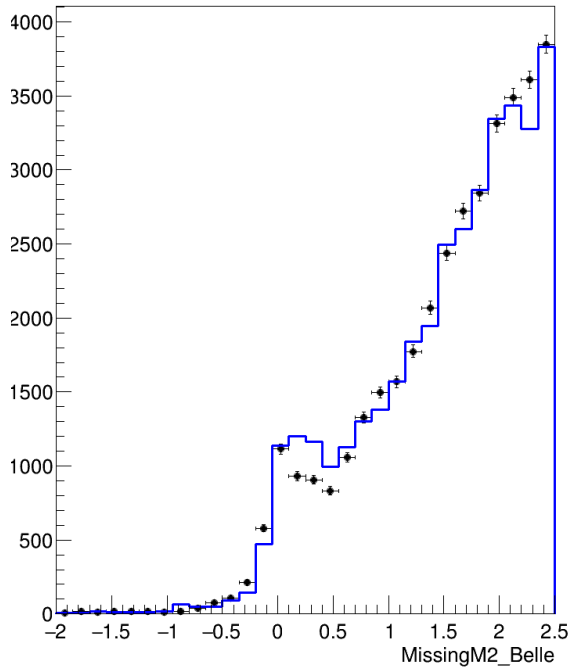

Figure 14: Fitting results. Data fitted is given in blue. The collective fitted PDF values are given in black. Fitting was done in 30 equal size bins in the interval [-2;2.5].

PDF	value	uncertainty
Signal	793	66
B background	33142	382
Continuum background	2540	330

Table 6.1: Fit results. All numbers have been rounded to integers.

	c1	c2	c3
c1	1.000	-0.196	0.064
c2	-0.196	1.000	-0.855
c3	0.064	-0.855	1.000

Table 6.2: Correlation matrix for the fitted coefficients.

Chapter 7

Results

In this chapter we present the fitting results as well as the Q^2 spectrum and discuss their consistency. The implications that arise and comparison to previous analyses is made in the chapter 9. The fitting results can be seen at the table 6.1 and at the plot 14. The pdf's used are presented at 13. The extracted q^2 spectrum is presented in in the figure 15. We estimate the goodness of the fit with $1 - P$, where P is the incomplete gamma function and it represents the probability, that the observed Chi-squared for a correct model should be less than the value chi2 that is being measured in this particular fit. We achieve a value of 0.989 for our fit.

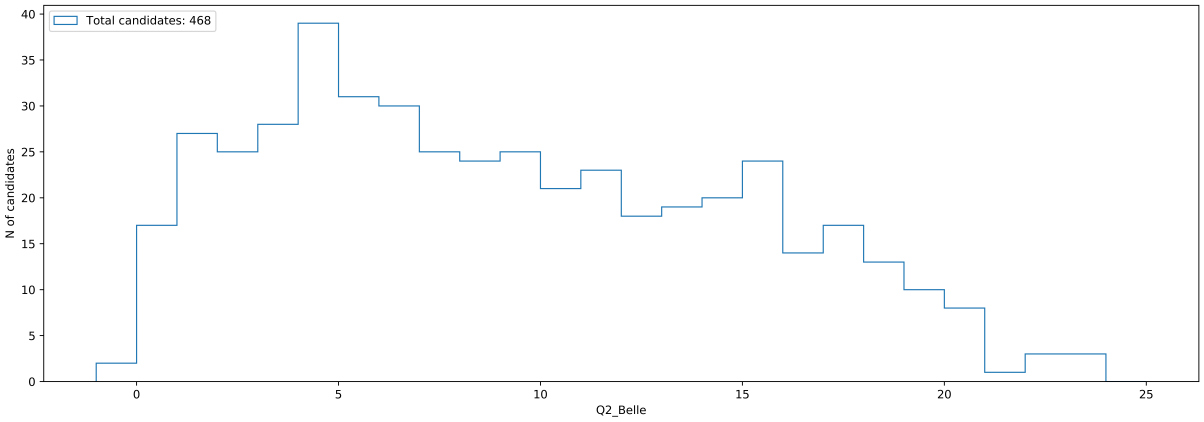

Figure 15: q^2 spectrum of the signal MC.

The shape of continuum pdf suggests, that in an attempt to filter out unnecessary events we came to the point, where statistical effects started playing quite a significant role, at least in this particular PDF. This could be

a source of uncertainty in the fit and can be avoided if one uses larger MC samples to produce PDFs. A small peak at 0 for B background PDF can be seen. It can be interpreted as stemming from wrongly reconstructed signal events and from cross-feed from other semileptonic decays, mainly $B \to \rho\ell\nu$, which has a similar topology to $B \to \pi\ell\nu$.

With the 1 ab^{-1} data the fitted number of signal candidates is 880±65. The expected number of the signal $B^0\bar{B}^0$ events that we analyse would be 5.35×10^8, number of signal events - 8.025×10^4 . The total efficiency can be calculated to be $1.15 \times 10^{-2} \pm 0.08$. We calculate the branching fraction as $\mathcal{B} = \frac{N_{sig.sel.}}{\epsilon N_{sig}}$, where the $N_{sig.sel}$ is the number of signal events in the sample selected from data with fitting after we did the reconstruction, ϵ - is the efficiency as calculated for the data sample, and N_{sig} is the total expected number of $B^0\bar{B}^0$ events. The branching fraction equals to $(1.43\pm0.10)\times10^{-4}$.

Chapter 8

Systematic uncertainties

Systematic uncertainties contribute to the overall uncertainty of the result. Being more precise, in the previous Belle analysis [16] the systematic uncertainty was of the same order as the statistical uncertainty. Therefore it is important to be able to determine the sources of systematic uncertainties, do a proper estimation and, of course, try to tackle them in future analyses. An analysis of systematic uncertainties for the results of this thesis has not been done. A general overview of systematics is presented in this chapter for completeness and further discussion. For the sake of brevity and consistency the description of the systematics is further heavily based on the results presented in the reference [16], as it is the most recent tagged exclusive decay reconstruction for our studied decay channel, that uses the FEI (or its predecessor FR) algorithm for the hadronic tag reconstruction.

Systematic uncertainties stem mostly from incorrect simulation of the physics of the detector and the physics of the particles overall. The sources relevant for the $\bar{B}^0 \to \pi^+ \ell^- \bar{\nu}_\ell$ mode, that were considered in the above-mentioned research are track reconstruction, lepton ID, FEI (FR) tagging efficiency, continuum description, description of cross-feed from other $B \to X_u \ell \nu$ decays and form factor shapes. Each separate contribution can be found at the table 8.1.The exact methods of estimation are described in the paper. Here we will further elaborate on the tag calibration uncertainty, as one sees, that it has a leading contribution to the systematics.

Error source	Relative uncertainty (%)
Track reconstruction	0.35
Lepton identificatioin	1.0
Kaon veto	0.9
Continuum description	1.0
X_u cross-feed	0.9
Tag calibration	4.5
Form factor shapes	1.1
Total	**5.0**

Table 8.1: Systematic uncertainties for branching fraction of $\bar{B}^0 \to \pi^+\ell^-\bar{\nu}_\ell$ decay from analysis[16].

8.1 FEI tagging calibration

FEI has been observed to have a larger efficiency on MC than on data. A separate study was made to estimate the efficiency correction factor. As in this thesis we do not directly operate with data, the FEI tag calibration has no effects on the immediate results themselves. However FEI is known to have a leading contribution in the systematic uncertainty of the results of previous analyses.

In general, the tag side is reconstructed with the FEI, the signal side is reconstructed in some chosen calibration decay mode. The calibration decay mode is ought to be well studied, so that all the major discrepancies between MC and data could be reasonably attributed to the tag-side reconstruction and FEI algorithm performance specifically. With a given signal decay channel the selection is done for data and MC. The yield of signal decays in data is then determined through fitting. The same expected yield is determined from MC directly. The correction factor is defined as a fraction of the yields: $\epsilon = N^{\text{Data}}/N^{\text{MC}}$. The exact variables used for fitting differ as do the reconstruction channels and selection methods. We will now give two specific examples.

For the Belle analysis[16] the calibration was done on $B \to X_c\ell\nu$ decay channels. As was mentioned before, FEI reconstructs the tag B in a list of defined decay channels. A single FEI channel was calibrated on a series of

separate exclusive charmed semileptonic decay channels, collectively written as $B \to X_c \ell \nu$. For a single FEI decay the calibration was averaged over those charmed decay channels. The variable used for fitting and extraction of the calibration factor was the missing mass squared.

The average correction factor for all the FEI channels was reported being roughly 0.75 and varying between different semileptonic modes due to tag- and signal-side interference. The breakdown of the total uncertainty for that analysis can be seen in the table 8.2. Statistical uncertainty is a common statistical uncertainty, since FEI are operating with statistical data. PDG branching fraction relates to the fact, that the current measured values for branching fractions also have uncertainties and these get propagated in the MC simulation. Particle ID selections were used for decay products, where $X_c = D^*$ was reconstructed, hence the D^* PID selection uncertainty.

Uncertainty source	Uncertainty (in%)
Statistical uncertainty	1.8
PDG branching fractions	2.5
D^* PID selection	3.0
Total	**4.5**

Table 8.2: Systematic uncertainties of the FEI calibration for B^0 channel from analysis[16].

Recently a separate study has been published[59] for the FEI tag calibration using Belle II data and MC. There for the purpose of calibration the inclusive semileptonic $B \to X \ell \nu$ decay was used (note that X is not necessarily a charmed meson as in previous case). For extraction of the calibration factor a fit to the lepton spectrum was performed.

For this case the tagging efficiency has been reported to depend on the cut on FEI signal probability. The results are presented at the table 8.3. Tagging efficiencies differ, as the signal B decay differences in reconstruction affect the selection. As one can try to infer, with our cut on the FEI signal probability being 0.005, the efficiency factor would roughly be 0.8 and the expected relative uncertainty on this factor would be around 5%.

Inclusive reconstruction for the calibration introduces a set of uncer-

FEI signal probability > 0.001	
Signal B decay	Tagging calibration factor
$\bar{B}^0 \to \pi^+ e^- \bar{\nu}_e$	0.83 ± 0.04
$\bar{B}^0 \to \pi^+ \mu^- \bar{\nu}_\mu$	0.83 ± 0.04
$\bar{B}^0 \to \pi^+ \ell^- \bar{\nu}_\ell$	0.83 ± 0.03
FEI signal probability > 0.01	
Signal B decay	Tagging calibration factor
$\bar{B}^0 \to \pi^+ e^- \bar{\nu}_e$	0.76 ± 0.04
$\bar{B}^0 \to \pi^+ \mu^- \bar{\nu}_\mu$	0.80 ± 0.04
$\bar{B}^0 \to \pi^+ \ell^- \bar{\nu}_\ell$	0.83 ± 0.03

Table 8.3: Calibration factors for FEI. In the original paper the channels are named according to tag B meson and signal lepton, e.g. $B^0 e^+$ for $\bar{B}^0 \to \pi^+ e^- \bar{\nu}_e$. The values written for general lepton decay channel are weighted averages of those for muon and electron channels. Correlations are taken into account.

tainties. The values are listed in the table 8.4. MC Stat. and Fit Stat. are statistical uncertainties of limited size of MC sample and fitting respectively. $\mathcal{B}(B^0 \to X\ell\nu)$ refers to the uncertainties in the PDG values that were used for MC simulation, which might have affected the $N^{\mathrm{MC}}_{X\ell\nu}$. Tracking and Lepton ID uncertainties are uncertainties associated with mismatches in reconstruction and particle identification between data and MC, which might have affected the $N^{\mathrm{MC}}_{X\ell\nu}$. $D\ell\nu$ FF and $D^*\ell\nu$ FF are the form factors uncertainties of the mentioned decays, which might have affected the $N^{\mathrm{MC}}_{X\ell\nu}$. In the reconstruction a cut is made on the lepton momentum ($p_\ell > 1$ GeV/c) and mismodelling of the form factors might change the $N^{\mathrm{MC}}_{X\ell\nu}$. Fit model refers to collective fitting systematic uncertainty connected primarily with the PDF having unknown shape. Eventually each of the abovementioned uncertainty sources contribute to the uncertainty of the PDF shape.

Channel	MC Stat.	$\mathcal{B}(B^0 \to X\ell\nu)$	Tracking	$D\ell\nu$ FF
$\bar{B}^0 \to \pi^+ e^- \bar{\nu}_e$	0.62	2.1	0.91	0.07
$\bar{B}^0 \to \pi^+ \mu^- \bar{\nu}_\mu$	0.6	2.09	0.91	0.06
	Lepton ID	$D^*\ell\nu$ FF	Fit Stat.	Fit Model
	0.73	0.43	1.22	3.72
	2.13	0.41	1.19	3.17

Table 8.4: Breakdown of uncertainty on the calibration factor for the selection FEI signal probability$>$ 0.001. The uncertainties are relative. Table copied from reference [59]. In the original paper the channels are named according to tag B meson and signal lepton, e.g. $B^0 e^+$ for $\bar{B}^0 \to \pi^+ e^- \bar{\nu}_e$

Chapter 9

Discussion

In the following chapter we will discuss the results and we will try to formulate expectations on possible results of the analysis with Belle II data. The latest analysis, that was doing an exclusive reconstruction of $\bar{B}^0 \to \pi^+ \ell^- \bar{\nu}_\ell$ decay with hadronic tagging at Belle is given in the reference [16]. We will be referring to this study throughout the chapter as "the Belle analysis" .

The fit that we performed had three free parameters and three components. As we outpointed this has led to some contamination of B background PDF with decays that also have peak at 0 in missing mass squared, such as $B \to \rho \ell \nu$. In the Belle analysis this was taken into account and a separate prediction for the amount of cross-feed from such decay was made. Also a separate PDF was made for modelling other $B \to X_u \ell \nu$ decays, see figure 16. However, coefficients scaling the PDF of continuum and decay to ρ meson were kept constant and were not fitted. One can expect that in Belle II with more statistics there will be a possibility to measure the cross-feed more precisely. Also with more data q^2 could be also measured with higher resolution, which would be interesting from the theoretical point of view.

The actual measured branching fraction $(1.43 \pm 0.10) \cdot 10^{-4}$ is in a relatively good agreement with the PDG value. Because we used MC as a data for analysis this is rather a consistency check. It simply means that our used method of measurement does not include any errors or biases by itself conceptually.

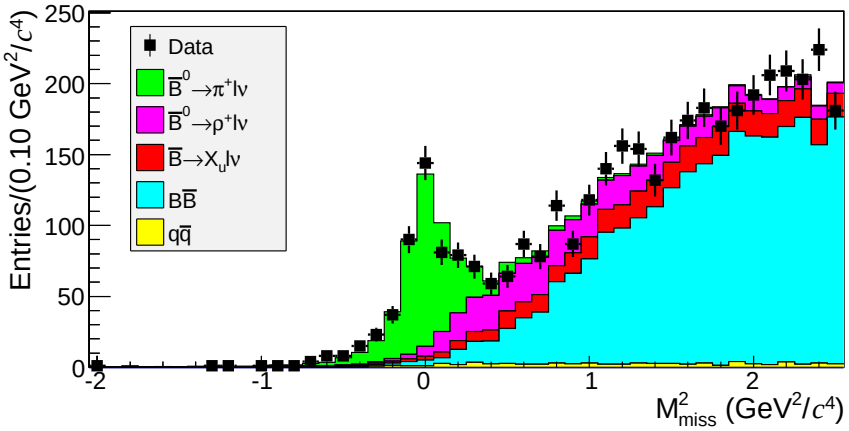

Figure 16: Fit to the missing mass squared distributions in data at Belle. The fit components are listed in the legend. Coefficients for continuum and ρ background were fixed.

The Belle analysis operated with a total of 772×10^6 $B\bar{B}$ events, which correspond to integrated luminosity of $711 fb^{-1}$. The branching fraction was calculated to be equal to $\mathcal{B}(\bar{B}^0 \to \pi^+ \ell^- \bar{\nu}_\ell) = (1.49 \pm 0.09 \pm 0.07) \times 10^{-4}$, where the first uncertainty is statistical and the second one is systematic. The total yield of signal events was 462.6 ± 27.7 with the efficiency of $2.07 \pm 0.02 \times 10^{-3}$.

The efficiency in our case is higher. This might be the consequence of improvement of FEI, as the Belle analysis was operating with it's predecessor FR. FEI gives a possibility to simultaneously account for multiple hadronic decay channels, but it relies heavily on the classifiers and their training, which introduce additional systematic uncertainties. Hence, one can expect the Belle II analysis to have a higher efficiency than in Belle. The exact behaviour of systematic uncertainties is discussed further in the chapter.

By straightforward scaling from yield and luminosity of the Belle analysis we can say that in Belle II analysis with planned 50 ab^{-1} of data one could expect the yield of signal events to be 33×10^3.

9.1 Precision

The statistical data uncertainty has been estimated from the amount of processed data. With Belle II expected to achieve an integrated luminosity of $50ab^{-1}$, 50 times higher than that of Belle, statistical uncertainty on the full Belle II data set should be roughly $\frac{0.09 \cdot 10^{-4}}{\sqrt{50}} \approx 0.0018 \cdot 10^{-4}$. With this the limiting precision would be the one of the systematic uncertainty.

The systematic uncertainty has many sources (see table 8.1 for the Belle analysis). The leading contribution comes from FEI calibration. FEI calibration in its turn operates with decay reconstruction (inclusive or exclusive) and essentially inherits uncertainties from which the reconstruction already suffers directly. This leads to a certain doubling of specific uncertainties, such as particle identification uncertainty, uncertainty of PDG values for measured branching fractions that are used in the MC production and so on. The semileptonic FEI calibration used in Belle has the uncertainty of of 4.5% and seems to be approximately as same effective as the new Belle II calibration [59], which has an uncertainty of 5.0%, see 8.2. However, the Belle II calibrations was trained only on a relatively small piece of data and is likely to improve.

An improvement that is likely to be made within Belle II analysis is the higher precision of the measured PDG values due to new experiments. This would leave the particle ID in the D^* determination the main source of systematic uncertainty in FEI tag calibration and correspondingly in the whole analysis. Since the Belle detector got upgraded one can expect the performance of the PID to improve. This statement, however, needs further validation and examination with the new data.

Overall, one can expect the new branching fraction measurement to have an uncertainty roughly 1.6 as low, at least because of the diminishing statistical uncertainty. $|V_{ub}|$ has PDG values 0.10 and 0.12 for experimental and theoretical uncertainties respectively. An improvement on branching fraction would lead to theoretical uncertainty playing the leading role.

The most precise determination published by the HFLAV[60] tries to

take into account known correlations between all previous measurements from all the different existing experiments and gives the value currently listed by the PDG. The total uncertainty on signal branching fraction and on the V_{ub} for such an average is an order of magnitude lower, than for a single measurement. The question about the anticipated Belle II measurement improving this result is yet to be considered as it depends equally on the improvements of the experiment and the theory.

Bibliography

[1] R. P. Feynman. "Mathematical Formulation of the Quantum Theory of Electromagnetic Interaction". In: *Phys. Rev.* 80 (3 Nov. 1950), pp. 440–457. DOI: 10.1103/PhysRev.80.440. URL: https://link.aps.org/doi/10.1103/PhysRev.80.440.

[2] D. Griffiths. *Introduction to Elementary Particles*. Physics textbook. Wiley, 2008. ISBN: 9783527618477. URL: https://books.google.de/books?id=Wb9DYrjcoKAC.

[3] J. C. Street and E. C. Stevenson. "New Evidence for the Existence of a Particle of Mass Intermediate Between the Proton and Electron". In: *Phys. Rev.* 52 (9 Nov. 1937), pp. 1003–1004. DOI: 10.1103/PhysRev.52.1003. URL: https://link.aps.org/doi/10.1103/PhysRev.52.1003.

[4] C.M.G. Lattes et al. "Processes involving charged mesons". In: *Nature* 159 (4047 1947), pp. 694–697. DOI: https://doi.org/10.1038/159694a0.

[5] C. S. Wu et al. "Experimental Test of Parity Conservation in Beta Decay". In: *Phys. Rev.* 105 (4 Feb. 1957), pp. 1413–1415. DOI: 10.1103/PhysRev.105.1413. URL: https://link.aps.org/doi/10.1103/PhysRev.105.1413.

[6] Steven Weinberg. "A Model of Leptons". In: *Phys. Rev. Lett.* 19 (21 Nov. 1967), pp. 1264–1266. DOI: 10.1103/PhysRevLett.19.1264. URL: https://link.aps.org/doi/10.1103/PhysRevLett.19.1264.

[7] G. Zweig. "An SU(3) model for strong interaction symmetry and its breaking. Version 1". In: (Jan. 1964).

[8] M. Gell-Mann. "The interpretation of the new particles as displaced charge multiplets". In: *Il Nuovo Cimento (1955-1965)* 4 (1956), pp. 848–866. DOI: https://doi.org/10.1007/BF02748000.

[9] W. Greiner et al. *Quantum Chromodynamics*. Springer Berlin Heidelberg, 2007. ISBN: 9783540485353. URL: https://books.google.de/books?id=iNev7iHHG%5C_MC.

[10] Georges Aad et al. "Observation of a new particle in the search for the Standard Model Higgs boson with the ATLAS detector at the LHC". In: *Phys. Lett. B* 716 (2012), pp. 1–29. DOI: 10.1016/j.physletb.2012.08.020. arXiv: 1207.7214 [hep-ex].

[11] Serguei Chatrchyan et al. "Observation of a New Boson at a Mass of 125 GeV with the CMS Experiment at the LHC". In: *Phys. Lett. B* 716 (2012), pp. 30–61. DOI: 10.1016/j.physletb.2012.08.021. arXiv: 1207.7235 [hep-ex].

[12] Rabindra N. Mohapatra and Goran Senjanovi ć. "Neutrino Mass and Spontaneous Parity Nonconservation". In: *Phys. Rev. Lett.* 44 (14 Apr. 1980), pp. 912–915. DOI: 10.1103/PhysRevLett.44.912. URL: https://link.aps.org/doi/10.1103/PhysRevLett.44.912.

[13] P.A. Zyla et al. "Review of Particle Physics". In: *Prog. Theor. Exp. Phys.* (2020).

[14] P. Gambino et al. "Challenges in Semileptonic B Decays". In: (June 2020). arXiv: 2006.07287 [hep-ph].

[15] Christopher Bouchard, Lu Cao and Patrick Owen. "Summary of the 2018 CKM working group on semileptonic and leptonic b-hadron decays". In: *10th International Workshop on the CKM Unitarity Triangle*. Feb. 2019. arXiv: 1902.09412 [hep-ex].

[16] A. Sibidanov et al. "Study of Exclusive $B \to X_u \ell \nu$ Decays and Extraction of $\|V_{ub}\|$ using Full Reconstruction Tagging at the Belle Experiment". In: *Phys. Rev. D* 88.3 (2013), p. 032005. DOI: 10.1103/PhysRevD.88.032005. arXiv: 1306.2781 [hep-ex].

[17] Kazunori Akai, Kazuro Furukawa and Haruyo Koiso. "SuperKEKB Collider". In: *Nucl. Instrum. Meth. A* 907 (2018), pp. 188–199. DOI: 10.1016/j.nima.2018.08.017. arXiv: 1809.01958 [physics.acc-ph].

[18] T. Abe et al. "Belle II Technical Design Report". In: (Nov. 2010). arXiv: 1011.0352 [physics.ins-det].

[19] Valerio Bertacchi et al. "Track Finding at Belle II". In: (Mar. 2020). arXiv: 2003.12466 [physics.ins-det].

[20] A. Bornheim et al. "Improved measurement of |V(ub)| with inclusive semileptonic B decays". In: *Phys. Rev. Lett.* 88 (2002), p. 231803. DOI: 10.1103/PhysRevLett.88.231803. arXiv: hep-ex/0202019.

[21] A. Limosani et al. "Measurement of inclusive charmless semileptonic B-meson decays at the endpoint of the electron momentum spectrum". In: *Phys. Lett. B* 621 (2005), pp. 28–40. DOI: 10.1016/j.physletb.2005.06.011. arXiv: hep-ex/0504046.

[22] Bernard Aubert et al. "Measurement of the inclusive electron spectrum in charmless semileptonic B decays near the kinematic endpoint and determination of |V(ub)|". In: *Phys. Rev. D* 73 (2006), p. 012006. DOI: 10.1103/PhysRevD.73.012006. arXiv: hep-ex/0509040.

[23] J.P. Lees et al. "Study of $\bar{B} \to X_u \ell \bar{\nu}$ decays in $B\bar{B}$ events tagged by a fully reconstructed B-meson decay and determination of $\|V_{ub}\|$". In: *Phys. Rev. D* 86 (2012), p. 032004. DOI: 10.1103/PhysRevD.86.032004. arXiv: 1112.0702 [hep-ex].

[24] Ilija Bizjak et al. "Determination of |V(ub)| from measurements of the inclusive charmless semileptonic partial rates of B mesons using full reconstruction tags". In: *Phys. Rev. Lett.* 95 (2005), p. 241801. DOI: 10.1103/PhysRevLett.95.241801. arXiv: hep-ex/0505088.

[25] P. Urquijo et al. "Measurement Of |V(ub)| From Inclusive Charmless Semileptonic B Decays". In: *Phys. Rev. Lett.* 104 (2010), p. 021801. DOI: 10.1103/PhysRevLett.104.021801. arXiv: 0907.0379 [hep-ex].

[26] J.P. Lees et al. "Measurement of the inclusive electron spectrum from B meson decays and determination of |Vub|". In: *Phys. Rev. D* 95.7 (2017), p. 072001. DOI: 10.1103/PhysRevD.95.072001. arXiv: 1611.05624 [hep-ex].

[27] Bernard Aubert et al. "Determinations of |V(ub)| from inclusive semileptonic B decays with reduced model dependence". In: *Phys. Rev. Lett.* 96 (2006), p. 221801. DOI: 10.1103/PhysRevLett.96.221801. arXiv: hep-ex/0601046.

[28] Bernard Aubert et al. "Determination of $|V_{ub}|$ from measurements of the electron and neutrino momenta in inclusive semileptonic B decays". In: *Phys. Rev. Lett.* 95 (2005). Ed. by R. Brenner, C.P. de los Heros and J. Rathsman. [Erratum: Phys.Rev.Lett. 97, 019903 (2006)], p. 111801. DOI: 10.1103/PhysRevLett.95.111801. arXiv: hep-ex/0506036.

[29] Robert V. Kowalewski and Sven Menke. "Complementary observables for the determination of |V(ub)| in inclusive semileptonic B decays". In: *Phys. Lett. B* 541 (2002), pp. 29–34. DOI: 10.1016/S0370-2693(02)02181-0. arXiv: hep-ex/0205038.

[30] Bernard Aubert et al. "Measurement of the CKM matrix element $|V_{ub}|$ with $B \to \rho e \nu$ decays". In: *Phys. Rev. Lett.* 90 (2003). Ed. by Patricia Ball et al., p. 181801. DOI: 10.1103/PhysRevLett.90.181801. arXiv: hep-ex/0301001.

[31] T. Hokuue et al. "Measurements of branching fractions and q**2 distributions for B —> pi l nu and B —> rho l nu decays with B —> D(*) l nu decay tagging". In: *Phys. Lett. B* 648 (2007), pp. 139–148. DOI: 10.1016/j.physletb.2007.02.067. arXiv: hep-ex/0604024.

[32] Bernard Aubert et al. "Measurement of the $B^+ \to \omega \ell^+ \nu$ and $B^+ \to \eta \ell^+ \nu$ Branching Fractions". In: *Phys. Rev. D* 79 (2009), p. 052011. DOI: 10.1103/PhysRevD.79.052011. arXiv: 0808.3524 [hep-ex].

[33] J.P. Lees et al. "Measurement of the $B^+ \to \omega \ell^+ \nu$ branching fraction with semileptonically tagged B mesons". In: *Phys. Rev. D* 88.7 (2013),

p. 072006. DOI: 10.1103/PhysRevD.88.072006. arXiv: 1308.2589 [hep-ex].

[34] J.P. Lees et al. "Branching fraction measurement of $B^+ \to \omega \ell^+ \nu$ decays". In: *Phys. Rev. D* 87.3 (2013). [Erratum: Phys.Rev.D 87, 099904 (2013)], p. 032004. DOI: 10.1103/PhysRevD.87.032004. arXiv: 1205.6245 [hep-ex].

[35] C. Schwanda et al. "Evidence for B+ —> omega l+ nu". In: *Phys. Rev. Lett.* 93 (2004), p. 131803. DOI: 10.1103/PhysRevLett.93.131803. arXiv: hep-ex/0402023.

[36] N.E. Adam et al. "A Study of Exclusive Charmless Semileptonic B Decay and |V(ub)|". In: *Phys. Rev. Lett.* 99 (2007), p. 041802. DOI: 10.1103/PhysRevLett.99.041802. arXiv: hep-ex/0703041.

[37] R. Gray et al. "A Study of Exclusive Charmless Semileptonic B Decays and Extraction of $|V_{ub}|$ at CLEO". In: *Phys. Rev. D* 76 (2007). [Addendum: Phys.Rev.D 76, 039901 (2007)], p. 012007. DOI: 10.1103/PhysRevD.76.012007. arXiv: hep-ex/0703042.

[38] P. del Amo Sanchez et al. "Study of $B \to \pi \ell \nu$ and $B \to \rho \ell \nu$ Decays and Determination of $|V_{ub}|$". In: *Phys. Rev. D* 83 (2011), p. 032007. DOI: 10.1103/PhysRevD.83.032007. arXiv: 1005.3288 [hep-ex].

[39] J.P. Lees et al. "Branching fraction and form-factor shape measurements of exclusive charmless semileptonic B decays, and determination of $|V_{ub}|$". In: *Phys. Rev. D* 86 (2012), p. 092004. DOI: 10.1103/PhysRevD.86.092004. arXiv: 1208.1253 [hep-ex].

[40] Bernard Aubert et al. "Measurements of $B \to \{\pi, \eta, \eta'\} \ell \nu_\ell$ Branching Fractions and Determination of $|V_{ub}|$ with Semileptonically Tagged B Mesons". In: *Phys. Rev. Lett.* 101 (2008), p. 081801. DOI: 10.1103/PhysRevLett.101.081801. arXiv: 0805.2408 [hep-ex].

[41] Bernard Aubert et al. "Measurement of the $B \to \pi \ell \nu$ Branching Fraction and Determination of $|V_{ub}|$ with Tagged B Mesons". In: *Phys. Rev.*

Lett. 97 (2006), p. 211801. DOI: 10.1103/PhysRevLett.97.211801. arXiv: hep-ex/0607089.

[42] D.J. Lange. "The EvtGen particle decay simulation package". In: *Nucl. Instrum. Meth. A* 462 (2001). Ed. by S. Erhan, P. Schlein and Y. Rozen, pp. 152–155. DOI: 10.1016/S0168-9002(01)00089-4.

[43] *Official EvtGen website*. URL: https://evtgen.hepforge.org/l.

[44] S. Jadach, B.F.L. Ward and Z. Was. "The Precision Monte Carlo event generator K K for two fermion final states in e+ e- collisions". In: *Comput. Phys. Commun.* 130 (2000), pp. 260–325. DOI: 10.1016/S0010-4655(00)00048-5. arXiv: hep-ph/9912214.

[45] S. Jadach, B.F.L. Ward and Z. Was. "Coherent exclusive exponentiation for precision Monte Carlo calculations". In: *Phys. Rev. D* 63 (2001), p. 113009. DOI: 10.1103/PhysRevD.63.113009. arXiv: hep-ph/0006359.

[46] Torbjorn Sjostrand, Stephen Mrenna and Peter Z. Skands. "A Brief Introduction to PYTHIA 8.1". In: *Comput. Phys. Commun.* 178 (2008), pp. 852–867. DOI: 10.1016/j.cpc.2008.01.036. arXiv: 0710.3820 [hep-ph].

[47] Andreas Moll. "The software framework of the Belle II experiment". In: *J. Phys. Conf. Ser.* 331 (2011). Ed. by Simon C. Lin, p. 032024. DOI: 10.1088/1742-6596/331/3/032024.

[48] S. Agostinelli et al. "Geant4—a simulation toolkit". In: *Nuclear Instruments and Methods in Physics Research Section A: Accelerators, Spectrometers, Detectors and Associated Equipment* 506.3 (2003), pp. 250–303. ISSN: 0168-9002. DOI: https://doi.org/10.1016/S0168-9002(03)01368-8. URL: http://www.sciencedirect.com/science/article/pii/S0168900203013688.

[49] J. Allison et al. "Geant4 developments and applications". In: *IEEE Transactions on Nuclear Science* 53.1 (2006), pp. 270–278.

[50] J. Allison et al. "Recent developments in Geant4". In: *Nuclear Instruments and Methods in Physics Research Section A: Accelerators, Spectrometers, Detectors and Associated Equipment* 835 (2016), pp. 186–225. ISSN: 0168-9002. DOI: https://doi.org/10.1016/j.nima.2016.06.125. URL: http://www.sciencedirect.com/science/article/pii/S0168900216306957.

[51] Thomas Keck. "The Full Event Interpretation for Belle II". MA thesis. KIT, Karlsruhe, Nov. 2014.

[52] T. Keck et al. "The Full Event Interpretation: An Exclusive Tagging Algorithm for the Belle II Experiment". In: *Comput. Softw. Big Sci.* 3.1 (2019), p. 6. DOI: 10.1007/s41781-019-0021-8. arXiv: 1807.08680 [hep-ex].

[53] Michael Feindt et al. "A Hierarchical NeuroBayes-based Algorithm for Full Reconstruction of B Mesons at B Factories". In: *Nucl. Instrum. Meth. A* 654 (2011), pp. 432–440. DOI: 10.1016/j.nima.2011.06.008. arXiv: 1102.3876 [hep-ex].

[54] Thomas Keck. "FastBDT: A Speed-Optimized Multivariate Classification Algorithm for the Belle II Experiment". In: *Comput. Softw. Big Sci.* 1.1 (2017), p. 2. DOI: 10.1007/s41781-017-0002-8.

[55] Geoffrey C. Fox and Stephen Wolfram. "Observables for the Analysis of Event Shapes in e+ e- Annihilation and Other Processes". In: *Phys. Rev. Lett.* 41 (1978), p. 1581. DOI: 10.1103/PhysRevLett.41.1581.

[56] A.J. Bevan et al. "The Physics of the B Factories". In: *Eur. Phys. J. C* 74 (2014), p. 3026. DOI: 10.1140/epjc/s10052-014-3026-9. arXiv: 1406.6311 [hep-ex].

[57] Dennis Weyland. "Continuum Suppression with Deep Learning techniques for the Belle II Experiment". PhD thesis. Karlsruhe Institute of Technology (KIT), 2017.

[58] Fons Rademakers et al. *root-project/root: v6.18/02*. Version v6-18-02. Aug. 2019. DOI: 10.5281/zenodo.3895860. URL: https://doi.org/10.5281/zenodo.3895860.

[59] F. Abudinén et al. "A calibration of the Belle II hadronic tag-side reconstruction algorithm with $B \to X\ell\nu$ decays". In: (Aug. 2020). arXiv: 2008.06096 [hep-ex].

[60] Y. Amhis et al. "Averages of b-hadron, c-hadron, and τ-lepton properties as of summer 2014". In: (Dec. 2014). arXiv: 1412.7515 [hep-ex].

Acknowledgement

I would like to thank Prof. Dr. Thomas Kuhr for his advices, corrections and guidance in doing this research. The possibility to do a short internship before the start of the thesis was very helpful and is very much appreciated.

I would very much like to thank Dr. Thomas Lueck for his immense input in shaping this research and its results, help with getting through the technicalities and thorough proofreading of the script.

Finally I would like to thank my fellow group members for their help and support.

Declaration of authorship

Declaration

I hereby declare that this thesis is a product of my own work and I have not used any sources or tools other than those stated in the thesis.

Erklärung:

Hiermit erkläre ich, die vorliegende Arbeit selbständig verfasst zu haben und keine anderen als die in der Arbeit angegebenen Quellen und Hilfsmittel benutzt zu haben.

München, 15.09.2020

Signature/Unterschrift